7th International Conference on Silicon Photovoltaics, SiliconPV 2017

Study of screen printed metallization for polysilicon based passivating contacts

Hande E. Çiftpınar[a,b], Maciej K. Stodolny[a], Yu Wu[a], Gaby J.M. Janssen[a], Jochen Löffler[a], Jurriaan Schmitz[c], Martijn Lenes[d], Jan-Marc Luchies[d], L.J. Geerligs[a]

[a]ECN Solar Energy, Westerduinweg 3, 1755 LE Petten, the Netherlands
[b]The Center for Solar Energy Research and Applications (GÜNAM), METU, Ankara, 06800, Turkey
[c]MESA+ Institute for Nanotechnology, University of Twente, P.O. Box 217, 7500 AE Enschede, The Netherlands
[d]Tempress Systems, Radeweg 31, 8171 MD Vaassen, The Netherlands

Abstract

We investigate contacting of n- and p-type polysilicon (polySi) passivating contact layers with industrial screen-printed metal pastes, examining both fire through (FT) and non-fire through (NFT) pastes. The n- and p-type polySi layers, deposited by low pressure chemical vapour deposition and doped by $POCl_3$ diffusion, phosphorus implant, or BBr_3 diffusion, result in excellent J_o, even for 50 nm thickness (<2 fA/cm^2 for n-polySi, <10 fA/cm^2 for p-polySi). The contact recombination is investigated by photoluminescence, and by cell test structures to determine V_{oc} as a function of metallization fraction. The contact resistance is investigated by transfer length method (TLM). The contacts are also extensively studied by high resolution electron microscopy. All-polySi solar cells (i.e., cells with front and back carrier selective layers consisting of polySi) are prepared. Excellent implied V_{oc} values of nearly 730 mV and 710 mV are obtained on the un-metallized polished and textured cells, respectively. The contact recombination after applying screen printed metallization can be analyzed well with both methods (PL and V_{oc}-based) rendering values for the prefactor of the recombination current $J_{o,c}$ at the contact areas of about 400 and 350 fA/cm^2 for 200 nm thick n-polySi and p-polySi, respectively.

Keywords: polysilicon; polySi; passivating contact; carrier selective contact; fire through metallization; contact recombination; contact resistance

1. Introduction

Passivating contacts [1] can solve a main remaining hurdle that limits the efficiency of current industrial n-type silicon solar cells: carrier recombination at the electrical contacts [2]. Introduction of passivating contacts to industrial solar cell processing is thus very appealing, but it is demanding at the same time. It requires the passivating properties to be stable when metallized with industrial fire through (FT) paste in a high temperature

firing step. One candidate for industrial passivating contacts is doped polysilicon (abbreviated as polySi in this article) on thin oxide [3], that has been shown to perform well at the rear side of PERPoly (Passivated Emitter Rear PolySilicon) solar cells metallized with industrial screen-print method [3], yielding in excess of 21% efficiency on 6 inch wafers [4].

In this paper, we study the contacting of polySi/SiO$_x$ structures by screen printed metallization, and we present and compare suitable analysis methods of contact recombination. N- and p-polySi layers with different thicknesses were prepared on thin oxide on polished and textured wafers, showing excellent surface passivation. The contact resistance of metallization by fire through (FT) and non-fire through (NFT) screen-printed pastes on these polySi layers is tested by transfer length method (TLM), for both polySi dopant types, to confirm a proper contact formation. The contact recombination (expressed as the prefactor $J_{o,c}$ of the contact recombination current) is quantified by photoluminescence (PL) measurements supported by device modelling, as well as by V_{oc} measurements for various metal contact fractions on all-polySi solar cells (i.e., cells with front and back carrier selective layers consisting of polySi). Finally, a detailed SEM study is carried out to image the contact structure.

2. Experimental

2.1. PolySilicon processing and metallization schemes

The passivating contact test structures and cells were fabricated on 6'' n-type solar grade Cz wafers, polished or textured, with a resistivity of 5 Ωcm. The thickness of chemically polished wafers was 160 μm and of textured wafers was 170 μm. Following the growth of a thin thermal oxide (Th.Ox), an intrinsic polySi layer was deposited with varying thicknesses (50, 75, 100, 125 and 200 nm) using low pressure chemical vapor deposition (LPCVD). For symmetrical samples the n-polySi layer was obtained by POCl$_3$ diffusion at 850°C, and p-polySi layers were obtained by BBr$_3$ diffusion at 880°C. For all-polySi cells (i.e., cells with front and back carrier selective Th.Ox/polySi stack) the n-type polySi was prepared by phosphorus implantation on one side (implant dose of 1E16 cm^{-2}, for 100 nm as well as 200 nm thickness) combined with an anneal provided by a BBr$_3$ diffusion at 880°C which also served as a doping source for creating p-polySi on the other side. The implant combined with BBr$_3$ diffusion resulted in n-poly and p-poly layers of similar doping levels as in the other experiments. The samples were characterized with electrochemical capacitance voltage (ECV) method for dopant profiles, and carrier lifetime measurements for implied V_{oc} (iV_{oc}) and passivation (J_o).

In order to investigate the impact of metallization on polySi properties, the polySi layers were contacted with industry-standard screen-printed fire through (FT) pastes, for contacting of phosphorus doped (Ag paste) or boron doped (AgAl paste) surfaces. Additionally, the samples with polished wafer surface were metallized with non-fire through (NFT) paste. Following glass removal and 80 nm SiN$_x$ deposition using plasma enhanced chemical vapour deposition (PECVD) on both surfaces of the samples, FT-Ag and FT-Ag/Al paste was printed on one side of n-poly/wafer/n-poly, p-poly/wafer/p-poly and n-poly/wafer/p-poly samples with various test patterns to evaluate contacting and passivating properties. Samples metallized with NFT paste were subjected to a SiN$_x$ patterning step prior to printing, to locally etch the SiN$_x$ layer and provide direct access of the NFT Ag paste to the underlying polySi layer. Curing of NFT paste was done at different temperatures within a 610-650°C range. Firing of the FT pastes was done at various temperatures within 745-825°C range to investigate the temperature-dependence of contact resistance and recombination of the metallized surfaces.

2.2. Contact resistance and contact recombination measurements

Contact recombination was analysed with two approaches: i) by modelling of PL maps (GreatEyes-LumiSolarCell, coupled/calibrated with Sinton PCD measurements), and ii) by V_{oc} measurements for various metal coverage fractions. In case i) the (average) PL signal over metallization patterns with different metal coverage, applied on one side of samples with the same layers of polySi on both sides, was used for extraction of $J_{o,c}$. In case ii), FT grids were applied on both sides of all-polySi cells, to obtain $J_{o,c}$ using V_{oc} measurements. Fig. 1 illustrates the different metal patterns. Fig. 1(a) shows the patterns printed on one side of symmetrical samples for PL imaging and modelling. A 2 mm pitch pattern of Fig. 1(a) was subsequently cut into strips for TLM measurements. Fig. 1(b) shows the PL image of samples with a V_{oc} test pattern consisting of small cells with various finger fractions of 2, 4, 8, 16, 25 and 32% (for finger widths varying from 60 to 190 μm and pitches from 2 down to 0.4 mm) applied on one side of all-polySi cells. An H-pattern locally interrupted with metal free regions was printed on the other side. In

addition to the test patterns, cells with on both sides a regular full-area H-pattern grid as shown in Fig. 1(c) were also prepared using the most promising temperature settings for firing/curing of the samples of Fig. 1(b). Contact resistivity (ρ_{co}) measurements were done using transfer length method (TLM, PVTools-TLM-SCAN).
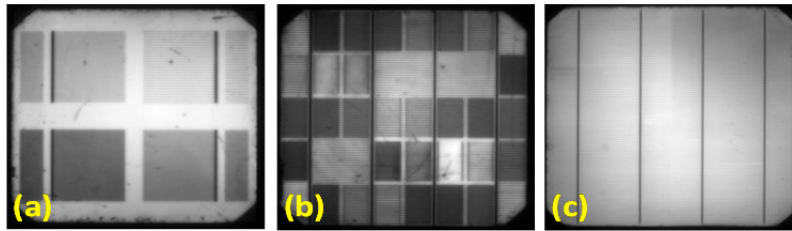

Fig. 1. PL images of textured wafers with 200 nm polySi passivating contacts, and printed FT metallization patterns. The metallization patterns consist of parallel fingers with varying pitches and widths. (a) 1-sided pattern used for PL analysis, 90 µm width fingers with pitches of 0.25, 0.5, 1 and 2 mm; (b) pattern with various metal fractions used for V_{oc} measurements; (c) pattern used for full-area cell metallization.

2.3. HR-SEM investigation of metallized polySi layers

Selected samples of all-polySi cells on polished and textured surfaces were sequentially repeatedly etched and imaged by high resolution scanning electroscope microscopy (HR-SEM), with top-view and cross-section images of the contacted and non-contacted areas after each etching step. As the first step of sequential etching, exposed (bulk) metal was etched using aqua regia (HNO_3:HCl, 1:3); followed by imaging, and a second etching step of glass removal using hydrofluoric acid (5% HF) solution. After second imaging, in the third etching step, all remaining Ag and Ag/Al nanoparticle-agglomerates were etched by aqua regia, followed by final imaging.

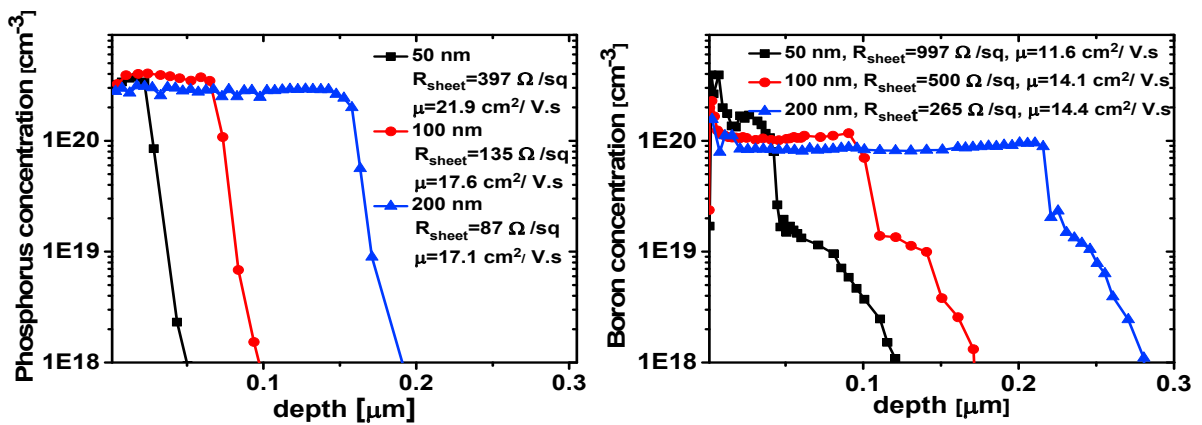## 3. Results and discussion

3.1. PolySi properties

Fig.2. Doping profiles for the phosphorus (a) and boron (b) doped polySi/SiOx/Cz-Si carrier selective contact layers with their corresponding R_{sheet} values, on polished wafers. The nominal thickness of the polySi layers before the doping was 50 nm, 100 nm and 200 nm.

Fig.2 shows the active phosphorus and boron concentration profiles, measured with ECV, for polySi layers of three different thicknesses, deposited on chemically polished wafers. The n-polySi layers resulting after $POCl_3$ diffusion were thinner than the nominal deposited thickness due to a consumption of polySi by phosphosilicate glass (PSG) formation, whereas p-poly layers preserved roughly the nominal thickness, with a boron rich layer (BRL) observed at the top surface. We have verified, by comparison of STEM/EDX [5] and ECV, that an abrupt drop in doping concentration defines the location of polySi/SiO$_x$ interface [4]. In the case of p-polySi the in-diffusion tails were substantial, which may be related to the higher temperature for B-diffusion compared to P-diffusion.

Increasing the layer thickness t_{poly} from 50 to 200 nm reduced the sheet resistance (R_{sheet}) of the n-polySi layer from 397 to 87Ω/□, and from 997 to 265Ω/□ for the p-polySi layer. The mobility values in Fig. 2 were calculated from $\mu = 1/(R_{sheet}.t_{poly}.N_D.q)$, with N_D the average dopant concentration and q the elementary charge, and are about 3-4x reduced compared to c-Si, both for n-poly and p-poly. The passivation properties of the layers are shown in Table 1 in terms of prefactor of the dark recombination current (J_o) [6], and in terms of implied V_{oc} (iV_{oc}).

Providing SiN$_x$ on both sides improved the iV_{oc} of all samples, with resulting highest values on polished samples of 744 mV for n-polySi and 725 mV for p-polySi, and corresponding J_o values of 0.6 fA/cm^2 and 7.3 fA/cm^2, respectively. Firing of the samples with PECVD SiN$_x$ coating layers improved the performance of the p-polySi layers, with a reduction of J_o by 15-30%. Firing has a slightly detrimental effect on n-polySi passivation which we believe is due to some other factors related to POCl$_3$ diffusion that we are presently investigating, for example (re-) injection of gettered impurities. The inferior passivation properties of p-poly compared to n-poly are not fully understood.

Table 1. Best passivation characteristics obtained on chemically polished 5 Ω.cm n-type Cz wafers. Symmetric wafer structure with P- or B-doped polySi/SiOx on both sides. Overall best values are printed in bold.

	thickness	with glass		SiNx-as deposited		SiNx+firing	
	(nm)	iV_{oc} (mV)	J_o (fA/cm^2)	iV_{oc} (mV)	J_o (fA/cm^2)	iV_{oc} (mV)	J_o (fA/cm^2)
n-poly	50	733	1.7	740	2.3	738	2.5
	100	731	**1.9**	744	**0.6**	742	**1.3**
	200	722	4.9	743	1.1	737	2.7
p-poly	50	707	**12.0**	724	7.8	728	6.2
	100	706	12.5	725	7.3	727	**5.1**
	200	705	12.8	726	**6.7**	728	5.7
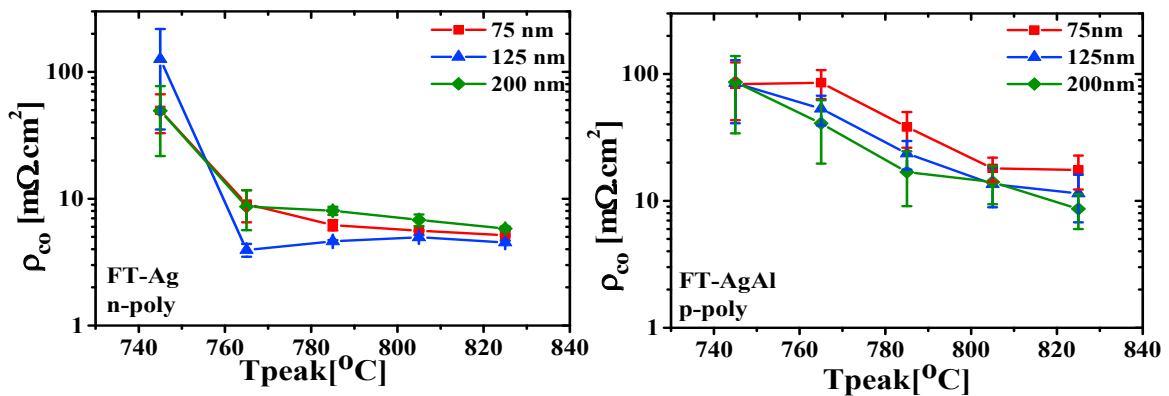
3.2. Contact resistance

Fig. 3. Contact resistivity ρ$_{co}$ of FT Ag paste on n-poly and AgAl paste on p-poly, on textured wafer surface, vs. firing temp (polySi is coated with SiN$_x$). Temperatures indicated are set points of peak temperature.

Fig. 3 shows contact resistivity ρ$_{co}$ of Ag FT paste on n-poly and AgAl FT paste on p-poly, in dependence on the set peak firing temperature. Starting from 785°C, the contact resistance is significantly reduced for both polySi polarities and above 800°C it becomes roughly constant, at around 3-5 and 9-12 mΩ.cm^2 for n- and p-polySi respectively. These values are to be compared to typical ρ$_{co}$ values of these pastes of 1-2 mΩ.cm^2 on n$^+$-diffused and 2-5 mΩ.cm^2 on p$^+$-diffused crystalline Si surfaces.

For the samples metallized with NFT paste on a polished wafer surface, TLM measurements of the contact on thin polySi layers (50 nm) resulted in ρ$_{co}$ > 3000 mΩ.cm^2 for n-polySi and > 100 mΩ.cm^2 for p-polySi, whereas on

thick (200 nm) layers values of ρ_{co} ~12 mΩ.cm^2 and ~26 mΩ.cm^2 were obtained for n-poly and p-poly, respectively. Improved contact resistivity on p-poly, down to ~9 mΩ.cm^2, was found on textured wafers. It should be noted that a dependence of ρ_{co} on the thickness or R_{sheet} of the polySi can be (partly) an artifact of the analysis method. The TLM analysis did not account for possible thinning of the polySi (resulting in an increase of the R_{sheet}) under the metallized finger, or for current pathways outside of the contacted polySi layer (which will depend on the polarity of the wafer). That means ρ_{co} could be overestimated [7].

3.3. Modelling of photoluminescence for extraction of $J_{o,c}$

The approach to PL modelling and extraction of $J_{o,c}$ from the PL measurements is to match Quokka [8, 9]-generated PL (*PLmod*) with experimental PL (*PLexp*), with $J_{o,c}$ as a variable. We use a Sinton PCD measurement to relate PL signal intensity to the surface passivation averaged over both sample surfaces ($J_{o,pas}$) prior to metallization. There are five different analysis locations on the samples as shown in Fig. 4.
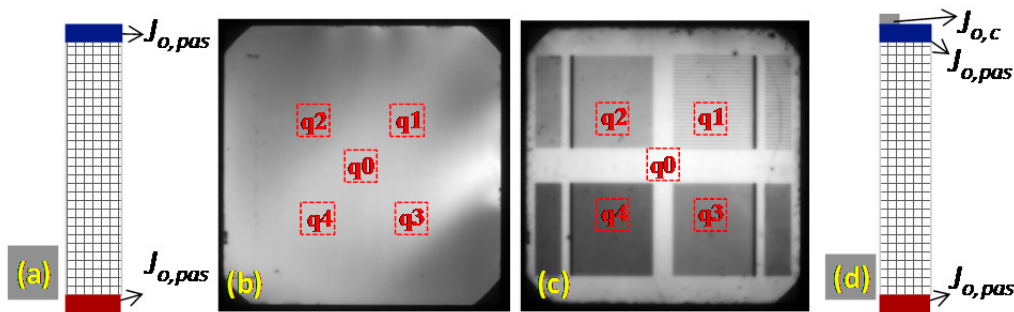

Fig. 4. Cross-sectional views of unit cells defined in Quokka before metallization (a) and after metallization+firing (d); PL images of symmetrical test structures before metallization (b) and after metallization+firing (c).

The sample before metallization is approximated by a symmetrical structure in Quokka as shown in Fig. 4(a), with the same R_{sheet} and $J_{o,pas}$ values for both surfaces, and with a fixed bulk lifetime of 3 ms. $J_{o,pas}$ is varied until modelled iV_{oc} is identical to measured one. Modelled $J_{o,pas}$ values were almost exactly the same as those obtained from Sinton PCD measurements. The PL emission in Quokka *(PLmod)* is used to calculate a calibration factor N that relates *PLmod* to the experimentally measured PL emission *PLexp* (locally, for each of the positions in Fig. 4(b)) as eq. (1).

$$N = \frac{PLmod}{PLexp} \tag{1}$$

N is subsequently used to relate *PLmod* to *PLexp* after metallization. Since the Sinton PCD measurement is no longer functional for the metallized regions [10], matching the Quokka-calculated PL emission with the experimental PL emission is used to find $J_{o,c}$.

Before extraction of $J_{o,c}$, an intermediate step is required to determine the effect of firing on passivation of non-metallized regions. Based on the results shown in Table 1, firing worsens passivation of non-metallized n-poly layers, while improving that of p-poly layers. For the PL samples after firing, the metal free region q0 in Fig. 4(c) is used to find $J_{o,pas}$ by matching *PLmod* and *PLexp*. The ratio of the two values of $J_{o,pas}$ obtained after and before firing is applied as correction factor to the $J_{o,pas}$ values in the modelling of the PL from the metallized regions q1-q4.

We have evaluated various approaches for extracting $J_{o,c}$ from modelling of PL measurements, with similar results. The approach presented here uses Quokka to model the area-averaged PL emission. In Quokka, an asymmetrical structure is defined using $J_{o,pas}$ (corrected for firing) for the whole rear side and the metal-free region on the front side, and $J_{o,c}$ for the metallized region on the front side. $J_{o,c}$ is determined so that the area-averaged PL emission in Quokka matches the measurement averaged over several fingers at some distance from the busbars. We have checked that variation of parameters for the PL emission model in Quokka have little effect on the outcome of

this modelling. The result of the above described procedure is given in Fig. 5 for three different polySi thicknesses on textured samples.

Increasing firing temperature increases contact recombination in all cases. The FT contacts on the thickest polySi layers generate contact recombination of only around 100-200 fA/cm^2. The $J_{o,c}$ of FT contacts on n-polySi is observed to be more sensitive to layer thickness than on p-polySi, and a $J_{o,c}$ value of 1400 fA/cm^2 is reached for nominal thickness of 75 nm n-polySi fired at 825°C, compared to around 400 fA/cm^2 for the equivalent p-polySi sample.
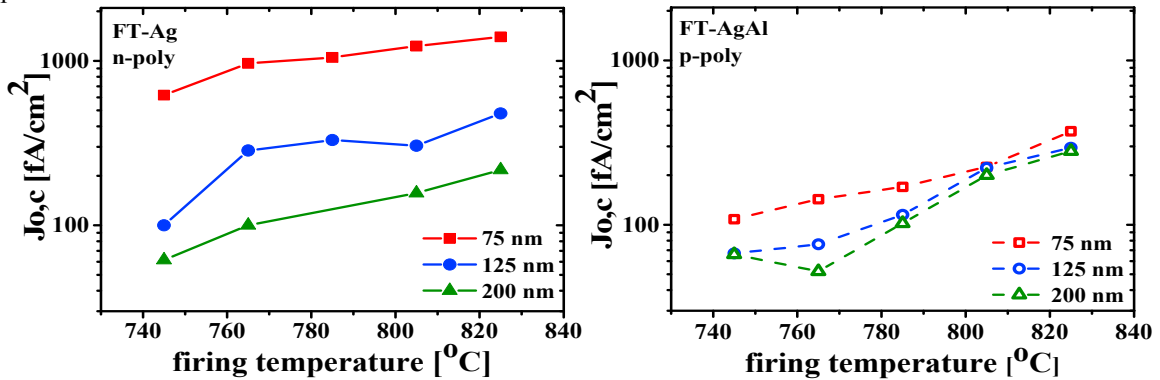

Fig. 5. Modelled $J_{o,c}$ for FT Ag paste on n-poly/wafer/n-poly (left) and FT AgAl paste on p-poly/wafer/p-poly (right) for 75, 125 and 200 nm poly layers fired at five different firing temperatures.

3.4. Extraction of $J_{o,c}$ from V_{oc} measurements

Metallization of all-polySi cells (cf. Fig. 2c) with FT paste resulted in a voltage loss of 30-40 mV relative to the iV_{oc} of the unmetallized half-fabricate, for both polished and textured cells. With NFT paste the observed voltage loss was around 20 mV. Results are summarized in Table 2. There is no clear advantage in V_{oc} for the thicker polySi compared to the thinner polySi. With the J_o values from the previous section, for the FT paste a reduction in V_{oc} of about 14 mV (200 nm) and 33 mV (100 nm) would have been expected, respectively.

Table 2. Measured best and average iV_{oc} (mV) and total $J_{o,pas}$ (fA/cm^2) for all-polySi half-fabricates, and the corresponding V_{oc} (mV) and FF (%) of best cells obtained with FT and NFT metallization for 100 and 200 nm thick polySi layers.

thick.	polished								textured							
	SiN$_x$ as depo.		SiN$_x$ + firing		FT+firing 785°C		NFT+curing		SiN$_x$ as depo.		SiN$_x$ + firing		FT+firing 785°C		NFT+curing	
	iV_{oc}	J_o	iV_{oc}	J_o	iV_{oc}	FF	iV_{oc}	FF	iV_{oc}	J_o	iV_{oc}	J_o	iV_{oc}	FF	iV_{oc}	FF
100	721	19	729	11	700	37	709	76.2	702	46	712	30	666	73	681	73.1
	705±17	47±34	715±15	30±21					699±2	51±3	709±2	33±3				
200	712	29	727	12	691	51	706	69.4	694	60	708	35	676	73	681	73.1
	701±8	39±8	722±6	16±4					689±4	66±7	704±4	39±5				

For further characterization of the contact recombination and comparison with the PL method, test cell patterns, as shown in Fig. 1b, with varying metal contact fractions were processed to quantify separately front and rear contact recombination. Measured V_{oc} values are translated into $J_{o,total}$ using the diode equation eq. (2).

$$V_{oc} = \frac{kT}{q} ln\left(\frac{J_{sc}}{J_{o,total}} + 1\right)$$

(2)

Then, $J_{o,c}$ is extracted from the slope of $J_{o,total}$ vs. metal area fraction, as shown in Fig. 6. Although the minimum finger area fraction was 2%, the two busbars per cell contribute 6.5% metal coverage, resulting in a minimum total metal fraction of 8.5%, increasing up to 38.5%. The busbars consisted of the same FT paste as the fingers, and it is

well known that busbar area contributes to recombination and V_{oc} loss due to metallization. However, the calculation of metal area fraction of the cell, where each cell area is defined as being delimited by the two busbars and the two outer fingers (see Fig. 1b) is somewhat arbitrary. For this reason, Fig. 6 only shows the results with finger metallization fraction of at least 8%, i.e total metal fraction larger than 14.5%. As seen in Fig. 6 (left), $J_{o,total}$ has a large standard deviation for the J_o-test pattern on the 100 nm thick poly layers, in particular the n-polySi layers. This could be related to the thinning of the n-poly layer during glass removal after diffusion, which could make the $J_{o,contact}$ on the thinnest n-poly very sensitive to small fluctuations in processing, e.g., firing temperature.

n-poly / Ag paste	thick. (nm)	Jo,c (fA/cm^2)
	100	1084±461
	200	386±22

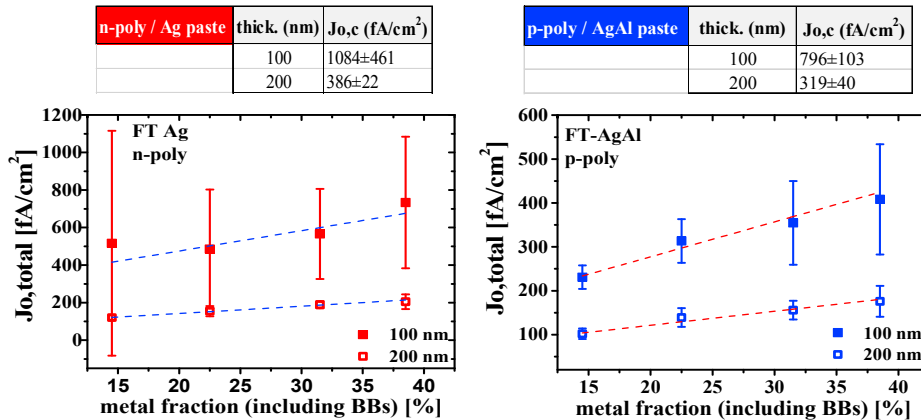| p-poly / AgAl paste	thick. (nm)	Jo,c (fA/cm^2)
	100	796±103
	200	319±40

Fig. 6. $J_{o,total}$ vs. metal fraction, and extracted $J_{o,c}$ values for nominally 100 and 200nm thick n-polySi, metallized with FT-Ag paste (left) and p-polySi metallized with FT-Ag/Al paste (right). Samples were fired with a set peak temperature of 825°C. The error margins are the standard deviation of the measurement of multiple cells with the same metal coverage on one wafer.

3.5. Comparison of $J_{o,c}$ obtained with different methods

The $J_{o,c}$ values from PL modelling of 1400, 480 and 220 fA/cm^2 for respective n-polySi thicknesses of 75, 125 and 200 nm fired with the peak temperature of 825°C, are comparable to the $J_{o,c}$ values of 1084±461 (for 100 nm) and 386±22 fA/cm^2 (for 200 nm) obtained from the V_{oc} measurements. The obtained $J_{o,c}$ values are somewhat higher than in earlier tests with n-polySi back contact on the PERPoly cells, where the contact recombination was estimated to be in the range of 100-200 fA/cm^2 for 200 nm n-polySi [3].

The V_{oc} measured for the nominally 100 nm thick p-polySi layers was observed to be less scattered compared to 100 nm thick n-poly layers, which could be related to the greater layer thickness, or less aggressiveness of the AgAl FT-paste. Less detrimental contacting of Ag/Al paste on p-polySi is also confirmed by the PL modelling results of $J_{o,c}$ of 400 and 250 fA/cm^2 for respective nominal thicknesses of 75 and 200 nm, compared to 796±103 and 319±40 fA/cm^2 from V_{oc} measurements.

Using the $J_{o,c}$ values obtained from the test structure analysis, the V_{oc} of full area all-polySi cells metallized with H-patterns on both surfaces was calculated to be 670±11 mV (100 nm polySi thickness) and 690±4 mV (200 nm polySi thickness). In contrast, the actual cell V_{oc} values were 666 mV and 676 mV for 100 and 200 nm polySi, respectively.

3.6. HR-SEM imaging of FT contacts on polySi

A detailed SEM study was carried out on the previously described samples with 100 nm polySi on textured wafers, metallized with FT paste and fired at 785 and 825°C. Fig. 7 shows images of samples that were processed first with aqua regia to remove the bulk of the metal paste, and subsequently with HF to remove the glass frit, leaving only the metal close to the wafer surface that was initially covered with glass frit. Fig. 7 additionally shows images of samples that were subsequently again processed with aqua regia to remove the final agglomerates of metal paste, showing the damage and pits resulting from intrusions of the paste into the wafer surface.

On sample cross sections of the n-polySi metallized with Ag FT paste, firstly it is striking that on large surface

areas the polySi layer appears to have been completely removed by the metallization paste, while in other areas it remained largely intact. For example, in Fig. 7 (b) no remaining polySi layer is visible, whereas Fig. 7(c) shows a transition between polySi-covered and bare areas. Metal intrusions into the c-Si wafer surface where the polySi layer was completely removed were observed for both 785 and $825^{\circ}C$ as seen in Fig. 7(a) and Fig. 7(d) respectively. Presence of metal in these intrusions was confirmed by back scattered electron (BSE) imaging. Applying aqua regia after HF etching made the damage on n-polySi better visible. Pits of ~100 nm diameter, distributed all over the polySi-free wafer surface, are observed in Fig. 7(b).

Lowering the firing temperature from $825^{\circ}C$ to $785^{\circ}C$ does not reduce the damage significantly: Ag agglomerates intrusion into the wafer and local removal of the n-polySi layer, are already present after firing at $785^{\circ}C$. SEM images of two samples fired at 785 and $825^{\circ}C$ taken with the same microscope settings were processed and analysed for pit area. Analysis showed that reducing firing temperature from 825 to $785^{\circ}C$ reduces pit area from 4.9 to 3.6% with corresponding $J_{o,c}$ drop from 480 to 330 fA/cm^2 shown in Fig. 5(left).
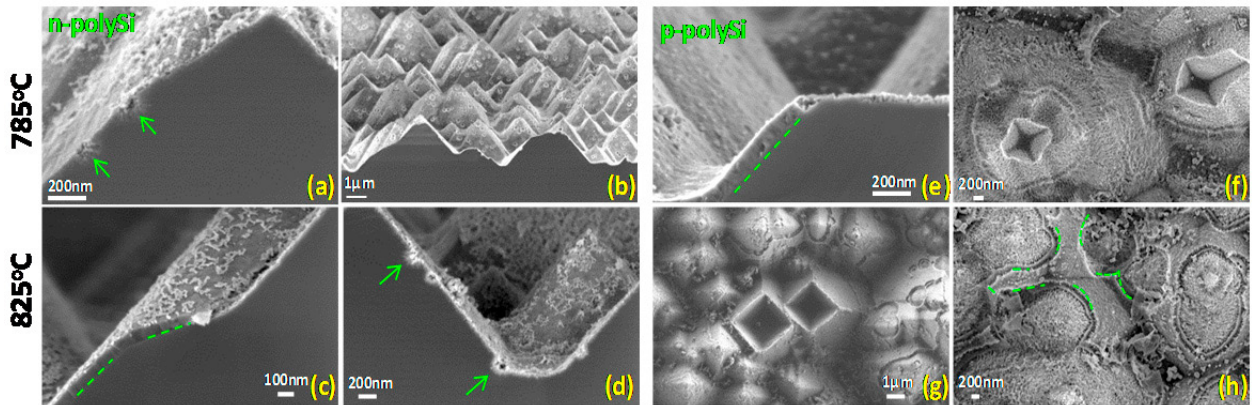

Fig. 7. High Resolution SEM investigation of polySi interaction with fire through pastes on textured surfaces. The samples have been processed first with aqua regia to remove the bulk of the metal paste, and subsequently with HF to remove the glass frit, leaving only the metal close to the wafer surface that was covered with glass frit (Fig. a,c,d,e). Subsequent further etching with aqua regia removed the last metal (Fig. b,f-h). The green dashed lines indicate the boundary polySi/wafer. Green arrows point at metal intrusions into the wafer.

As shown in Fig. 7(e), cross-section analysis of the p-poly side of the same samples after glass removal revealed that local removal of the polySi layer also happens for p-polySi, even after firing at the lowest temperature ($785^{\circ}C$). The p-polySi layer is typically removed from the texture pyramid tips, whereas it is often still present intact in the valleys between the texture pyramids. Top-view analysis also showed the existence of large pits with inverted pyramid shape with (111) facets at the tips of some texture pyramids (Fig. 7(f)), indicating that Si is replaced by metal that grows into Si [11]. Removing remaining Ag/Al particle agglomerates using aqua regia visualizes the extent of damage to the polySi layer and the underlying c-Si surface. Fig. 7(h) shows that where the polySi layer is removed the underlying c-Si surface is damaged. Increasing the firing temperature from 785 to $825^{\circ}C$ promotes the formation of the inverted pyramids at the tips of texture pyramids, as seen in Fig. 7(g). This coincides with reduced ρ_{co} as observed in Fig. 3 (right) and increased recombination losses in Fig. 6. The recombination losses of p-polySi contacted with FT-Ag/Al paste increase as a function of increasing firing temperature with only a slight dependence on layer thickness.

3.7. HR-SEM imaging of NFT contacts on polySi

All-polySi cells metallized with NFT paste on polished wafers were analysed by SEM following the removal of bulk metal using aqua regia. Small openings and locally thinned regions were observed on both n-poly and p-poly side of the samples as seen in Fig. 8. Unlike FT paste, no extensive etching of poly layer was observed for NFT paste other than small shallow openings. This should be favorable for a passivating contact structure.
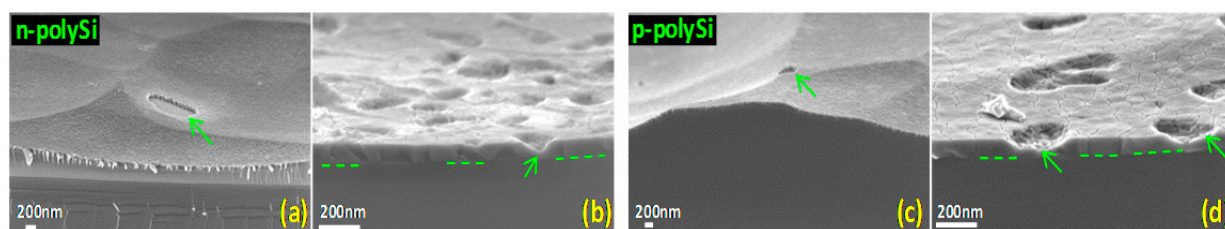
Fig. 8. High Resolution SEM investigation of polySi interaction with non-fire through pastes on polished surfaces. The green dashed lines indicate the boundary polySi/wafer. Green arrows point local damages on polySi layer.

The gentler contacting mechanism of NFT paste was expected to suppress contact recombination losses. However, samples metallized with NFT paste still show a significant V_{oc}-loss at cell level as shown in Table 2. Possible explanations include hydrogen effusion during curing of the paste (patterning of SiNx prior to printing created wider openings than printed finger width), or a detrimental metal-polySi interaction. However, curing of samples with patterned SiN_x but without NFT paste did not show any degradation. Therefore, the degradation is more likely affected by some kind of local damage to the polySi layer or metal-polySi interaction.

3.8. Contact formation of FT paste on polySi

The SEM images suggest that contact formation of FT-Ag paste on n-polySi layers is based on either i) Ag nanoparticle agglomerates on the remaining areas of n-polySi layer, or ii) intrusions of Ag into the wafer where the n-polySi layer has disappeared. Given the removal of large areas of n-polySi layer the relatively low $J_{o,c}$ is perhaps surprising, and suggests some passivation from frit and/or an effect of surface doping from the phosphorus in the dissolved n-poly. To understand the contact and passivation mechanism better, SEM characterisation as presented should be conducted for increased polySi layer thickness

The SEM images suggest that contacting of FT-AgAl on p-poly is by either i) the large inverted pyramids, ii) Ag nanoparticle agglomerates on the wafer where the p-polySi layer was removed, or iii) Ag nanoparticle agglomerates on the p-polySi layer where it was not removed. Considering the very high ρ_{co} values of p-polySi measured on polished wafers, it is likely that i) is the main mechanism for the contacting of p-polySi layers. In Fig. 7(f, g) increasing firing temperature was observed to increase the depth and width of the inverted pyramids, which is consistent with improved ρ_{co} as a function of increasing firing temperature shown in Fig. 3(right). Since these inverted pyramids penetrate several microns deep into the underlying Si wafer [13], there is no thickness dependence of ρ_{co}. These inverted pyramids do not shunt the emitter, which probably is as a result of high acceptor concentration at the interface with the wafer [15]. Their area coverage is only about 1% [16] of the metallized region which is enough to form a proper contact and which results in lower $J_{o,c}$ compared to the Ag paste on n-polySi layers. Also, a large fraction of the rest of the surface under the printed metal contact is still passivated by the remaining p-polySi layer.

4. Conclusions

We presented studies of both p-type and n-type polysilicon passivating contacts and their metallization with industrial fire through (FT) screen printed pastes. The carrier selective polySi/SiO$_x$ passivating contact layers were produced with an LPCVD based polySi deposition process on both sides of 6 inch Cz wafers. The polySi/SiO$_x$ passivating layers, with thickness down to 50 nm, resulted in very low J_o. The FT metal contacted polySi was analysed in terms of contact resistivity, contact recombination and resulting cell performance, for different polySi thicknesses, and pastes fired at various temperatures. Contact recombination was analysed both by using a newly-developed modelling procedure based on QSSPC-calibrated PL measurements, and by means of V_{oc} measurements for various metal fractions. Results from both methods were in approximate agreement, with $J_{o,c}$ around 400 (1400) and 350 (800) fA/cm^2 for n-polySi and p-polySi layers of 200 (100) nm thickness. HR-SEM imaging of contacted regions strikingly revealed that the FT-metallization locally removed large fractions of the polySi layer, and damaged the underlying substrate, by means of mainly Ag intrusions on the n-polySi contacted with industrial Ag

paste, and Al-based inverted pyramids on the p-polySi contacted with industrial AgAl paste. The SEM images combined with other results also hinted at possible mechanisms and pathways for the electronic contact. The Al-based inverted pyramids are likely the main contributor for the contacting of p-polySi layers. Considering that conventional FT metallization on high performance (low doped) homojunctions results in $J_{o,c}$ of about 2500 fA/cm^2 [17], the $J_{o,c}$ determined on the polySi layers of 200 nm thickness is already an order of magnitude lower, with resulting significant benefit for cell V_{oc}. To have full benefit of the excellent low J_o of the non-contacted polySi areas, further work needs to be done to strongly reduce $J_{o,c}$ of FT metallization in particular for the thinnest polySi layers. A companion paper at this conference reports recent progress on FT contacting on n-polySi [5] showing that very low $J_{o,c}$ can be achieved also on 100 nm thick polySi.

Acknowledgments

References

[1] P. Stradins, A. Rohatgi, S. Glunz, J. Benick, F. Feldmann, S. Essig, W. Nemeth, A. Upadhyaya, B. Rounsaville, Y.-W. Ok, B. Lee, D. Young, A. Norman, Y. Liu, J.-W. Luo, E. Warren, A. Dameron, V. LaSalvia, M. Page and M. Hermle, "Passivated tunneling contacts to n-type wafer silicon and their implementation into high performance solar cells," in *WCPEC-6: 6th World Conference on Photovoltaic Energy Conversion*, Kyoto, Japan, 2014.

[2] F. Feldmann, M. Bivour, C. Reichel, M. Hermle and S. W. Glunz, "Passivated rear contacts for high-efficiency n-type Si solar cells providing high interface passivation quality and excellent transport characteristics," *Solar Energy Materials and Solar Cells,* no. 120, pp. 270-274, 2014.

[3] E. Yablonovitch, R. M. Swanson and Y. H. Kwark, in *Proceedings of the 17th IEEE Photovoltaic/Spec. Conf.*, 1984.

[4] M. Stodolny, M. Lenes, Y. Wu, G. Janssen, I. Romijn and J. Luchies, "n-Type polysilicon passivating contact for industrial bifacial n-type solar cells," *Solar Energy Materials and Solar Cells,* no. 158, pp. 24-28, 2016.

[5] M. Stodolny, L. Geerligs, G. Janssen, B. van de Loo, J. Melskens, R. Santbergen, O. Isabella, J. Schmitz, M. Lenes, J. Luchies and W. Kessels, "Material properties of LPCVD Processed n-type Polysilicon Passivating Contacts and Application in PERPoly Industrial Bifacial Solar Cells," in *Energy Procedia*, Freiburg, Germany, 2017.

[6] B. Thuilier, J. Boyeaux, A. Kaminski and A. Laugier, "Transmission electron microscopy and EDS analysis of screen-printed contacts formation on multicrystalline silicon solar cells," *Materials Science and Engineering:B,* vol. 102, no. 1-3, pp. 58-62, 2003.

[7] D. Kane and R. Swanson , "Measurement of the emitter saturation current by a contactless photoconductivity decay method," in *18th IEEE Photovoltaic Specialists Conference, Las Vegas: 1985. p. 578.*.

[8] S. Eidelloth and R. Brendel, "Analytical Theory for Extracting Specific Contact Resistances of Thick Samples From the Transmission Line Method," *IEEE ELECTRON DEVICE LETTERS,* vol. 35, no. 1, pp. 9-11, 2014.

[9] A. Fell, "A Free and Fast Three-Dimensional/Two-Dimensional Solar Cell Simulator Featuring Conductive Boundary and Quasi-Neutrality Approximations," *IEEE TRANSACTIONS ON ELECTRON DEVICES,* vol. 60, no. 2, pp. 733-738, 2013.

[10] A. Fell, K. McIntosh, M. Abbott and D. Walter, "Quokka version 2: selective surface doping, luminescence modeling and data fitting," in *23rd Photovoltaic Science and Engineering Conference (PVSEC)*, Taipei, 2013.

[11] J. Deckers, X. Loozen, N. Posthuma, B. O'Sullivan, M. Debucquoy, S. Singh, M. Aleman, M. Payo, I. Gordon, P. Verlinden, R. Mertens and J. Poortmans, "Injection dependent emitter saturation current density measurement under metallized areas using photoconductance decay," in *28th European Photovoltaic Solar Energy Conference and Exhibition*, 2013.

[12] S. Fritz, M. König, S. Riegel, A. Herguth, M. Hörteis and G. Hahn, "Formation of Ag/Al Screen Printing Contacts on B Emitters," *IEEE Journal of Photovoltaics,* vol. 5, no. 1, pp. 145-151, 2015.

[13] S. Fritz, S. Riegel, A. Herguth and G. Hahn, "Influence of Si surface orientation on screen-printed Ag/Al contacts," in *5th International Conference on Silicon Photovoltaics, SiliconPV 2015*, Konstanz, Germany, 2015.

[14] W. Wu, K. E. Roelofs, S. Subramoney, K. Lloyd and L. Zhang, "Role of aluminum in silver paste contact to boron-doped silicon emitters," *AIP Advances,* vol. 7, no. 015306, 2017.

[15] S. Riegel, F. Mutter, T. Lauermann, B. Terheiden and G. Hahn, "Review on screen printed metallization on p-type silicon," in *3rd Workshop on Metallization for Crystalline Silicon Solar Cells: Energy Procedia*, Charleroi, Belgium, 25-26 October, 2011.

[16] N. Wöhrle, E. Lohmüller, S. Werner and J. Greulich, "Development, Characterization and Modelling of Doping Profile, Contact Resistance and Metal Spiking in Diffused and Screen-Printed Boron Emitters," in *31st European PV Solar Energy Conference and Exhibition*,

Hamburg, Germany, 14-18 September, 2015.

[17] B. Geerligs, M. Stodolny, Y. Wu, A. Gutjahr, G. Janssen, I. Romijn, J. Anker, E. Bende, H. Ciftpinar, M. Lenes and J. M. Luchies, "LPCVD polysilicon passivating contacts," in *Workshop on Crystalline Silicon Solar Cells and Modules: Materials and Processes*, Vail, Co., USA, 28 - 31 August 2016.

[18] E. Cabrera, S. Olibet, J. Glatz-Reichenbach, R. Kopecek, D. Reinke and G. Schubert, "Current transport in thick film Ag metallization: Direct contacts at Silicon pyramid tips?," in *Energy Procedia*, Freiburg, Germany, 2011.

[19] S. Sze, Semiconductor Devices: Physics and Technology, John Wiley & Sons Inc., 1998.

[20] E. Cabrera, S. Olibet, D. Rudolph, P. E. Vullum, R. Kopecek, D. Reinke, C. Herzog, D. Schwaderer and G. Schubert, "Impact of excess phosphorus doping and Si crystalline defects on Ag crystallite nucleation and growth in silver screen-printed Si solar cells," *Progress in Photovoltaics: Research and Applications,* vol. 23, pp. 367-375, 2015.

[21] D. Meier, E. Good, R. Garcia, B. Bingham, S. Yamanaka, V. Chandrasekaran and C. Bucher, "DETERMINING COMPONENTS OF SERIES RESISTANCE FROM MEASUREMENTS ON A FINISHED CELL," in *IEEE 4th World Conference on Photovoltaic Energy Conference*, Waikoloa HI, USA, 2006.